Aji, Arif T.; Aromaa, Jari; Lundström, Mari

The optimum electrolyte parameters in the application of high current density silver electrorefining

Published in:
Metals

DOI:
10.3390/met10121596

Published: 01/12/2020

Document Version
Publisher's PDF, also known as Version of record

metals

MDPI

Article

The Optimum Electrolyte Parameters in the Application of High Current Density Silver Electrorefining

Arif T. Aji, Jari Aromaa and Mari Lundström *

Department of Chemical and Metallurgical Engineering, School of Chemical Engineering, Aalto University, P.O. Box 16200, FI 00076 Aalto, Finland; arif.aji@aalto.fi (A.T.A.); jari.aromaa@aalto.fi (J.A.)

* Correspondence: mari.lundstrom@aalto.fi

Received: 5 October 2020; Accepted: 24 November 2020; Published: 28 November 2020

Abstract: Increasing silver production rate has been a challenge for the existing refining facilities. The application of high current density (HCD) as one of the possible solutions to increase the process throughput is also expected to reduce both energy consumption and process inventory. From the recently-developed models of silver electrorefining, this study simulated the optimum electrolyte parameters to optimize the specific energy consumption (SEC) and the silver inventory in the electrolyte for an HCD application. It was found that by using $[Cu^{2+}]$ in electrolyte, both objectives can be achieved. The suggested optimum composition range from this study was $[Ag^{+}]$ 100–150 g/dm^3, $[HNO_3]$ 5 g/dm^3, and $[Cu^{2+}]$ 50–75 g/dm^3. HCD application (1000 A/m^2) in these electrolyte conditions result in cell voltage of 2.7–3.2 V and SEC of 0.60–1.01 kWh/kg, with silver inventory in electrolyte of 26–39 kg silver for 100 kg per day basis. The corresponding figures for the conventional process were 1.5–2.8 V, 0.44–0.76 kWh/kg, and 15.54–194.25 kg, in respective order. These results show that, while HCD increases SEC by app. 30%, the improvement provides a significant smaller footprint as a result of a more compact of process. Thus, applying HCD in silver electrorefining offers the best solution in increasing production capacity and process efficiency.

Keywords: high current density; silver electrorefining; energy consumption

1. Introduction

Silver is used in many applications such as coins, jewelry, medicine, dentistry, plating, electrical technology, chemical equipment, catalyst, and photography [1]. The recorded production of silver from 1950 to 2018 shows a linear trend with an increasing rate of approximately 300 tons of silver product per year as can be seen in Figure 1a [2]. In order to meet the increasing demand, increase in the existing capacity or higher kinetics of processing is required. Accordingly, developments in the existing silver electrorefining process were more focused on the increase of processing rate, reduction of metal inventory, and increase of metal recovery rate [3]. One of the developments was high current density (HCD), or the application of current density over 1000 A/m^2 silver electrorefining, which offers a logical solution for the increasing capacity demand. Started in 1980 in Sweden, this process development path has recorded 11 installations of HCD silver electrorefining worldwide until 2014 [4]. Furthermore, the reported- and published research and development of the process shows that recent investigations [4–10] were focused on the implementation of higher current density as shown by Figure 1b, making it the most renowned improvement in the recent years.

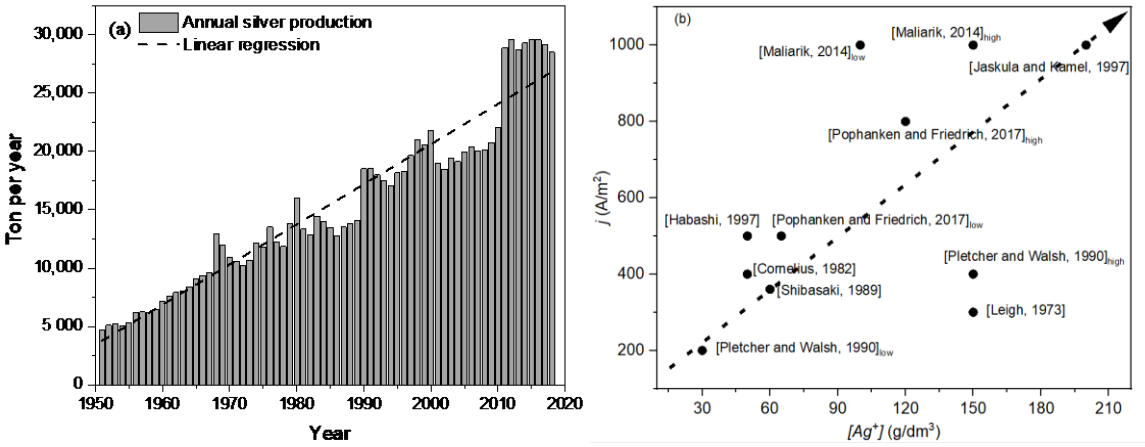

Figure 1. (**a**). Annual production of silver in the period of 1950–2018 [2] and (**b**) published studies on silver electrorefining showing the correlation of current density to the concentration of silver in the electrolyte [1,4–10].

Similar to the conventional electrorefining, HCD silver electrorefining uses cast anodes and $AgNO_3$-HNO_3 electrolyte with the arrangement of Moebius cell [4]. Nevertheless, the processes difference in electrolyte parameters. Conventional process uses $[Ag^+]$ = 40–150 g/dm^3 (as $AgNO_3$) [1,6–12] while the HCD process uses higher concentrations of $[Ag^+]$ = 100–150 g/dm^3 in the electrolyte [4]. In conventional silver electrorefining free acid $[HNO_3]$ is within the range of 0–10 g/dm^3 [8], meanwhile for HCD, even though it is not clearly stated, the electrolyte should be less acidic with pH > 2 [4,5]. With the assumption that HNO_3 is the only pH regulator, the pH > 2 values correspond to $[HNO_3]$ of lower than 0.63 g/dm^3. Thus, the electrolyte of HCD has higher $[Ag^+]$ and lower $[HNO_3]$ in comparison to the conventional process. The high $[Ag^+]$ in electrolyte increases the Ag inventory, being one of the disadvantages of the HCD application.

Another distinct difference of the conventional and HCD process is the current density with conventional silver electrorefining current density is within the range of 200–800 A/m^2 as shown in Table 1 [1,5–9,12] whereas the HCD current density targets to 1000 A/m^2 [4,5]. As shown in the same table, conventional cell voltage within the range of 1.5–2.8 V [1,7,8] leads to specific energy consumption of 0.6–0.8 kWh/kg [11,12]. Meanwhile, HCD cell voltage is approximately 5 V [4] which equal to 1.27 kWh/kg. This higher energy consumption of the silver electrorefining process is another disadvantage of the application of HCD.

Table 1. Conventional silver electrorefining process parameters.

Parameters	[1]	[5]	[6]	[7]	[8]	[9]	[12]
$[Ag^+]$	50	150–200	65–120	150	30–150	50	50
$[HNO_3]$	10	2.5	0.6–10	2–6.2 *	0–10	-	10
T (°C)	-	35–50	35	32	25	45	-
$wt\%_{Ag}$ (%)	95	99.3	96.5	86–92	86–92	98	>99
$wt\%_{Au}$ (%)	4	0.04–0.07	0.01	8–9	8–9	0.5	-
$wt\%_{Cu}$ (%)	1	0.4–0.6	3	0.5–1	0.5–1	1	-
j (A/m^2)	400–500	1000	500–800	300 #	200–400	400	400–500
V_{cell} (V)	2.0–2.5	-	-	2.7	1.5–2.8	-	2.0–2.5

* calculated from the pH information, and # was unit conversion from amps/sq feet.

At the current state of increasing industrial demand, improvement to the process throughput is getting more important than ever before. On the other hand, the conventional silver electrorefining process itself has a very wide range of operating parameters. Thus, optimization for the process is required to take into account both opportunity of improvements of increasing the process throughput and to have well-designed process parameters for an optimal process.

The disadvantages of high cell voltage and high energy consumption of the HCD application in comparison to the conventional process consequently raised a question of whether HCD could be adapted in the existing silver electrorefining to increase the productivity. The process integration probably has been the cause for the low implementation of HCD from the time it was introduced almost four decades ago. In this investigation, the decisive parameters for the HCD application are defined for the optimum silver electrorefining process based on the current industrial conditions.

2. Methods

Investigation on the applicability of HCD process to silver electrorefining is conducted through the simulation of the published models as shown by Figure 2. The models in consideration are regression models from the following publications:

a. Empirical model of electrolyte conductivity as a function of electrolyte concentrations and temperature [13].
b. Silver dissolution as a function of electrolyte concentrations and temperature [14].
c. Effect of Au content in anode due to anode passivation [15].
d. Electrode overpotential [16].

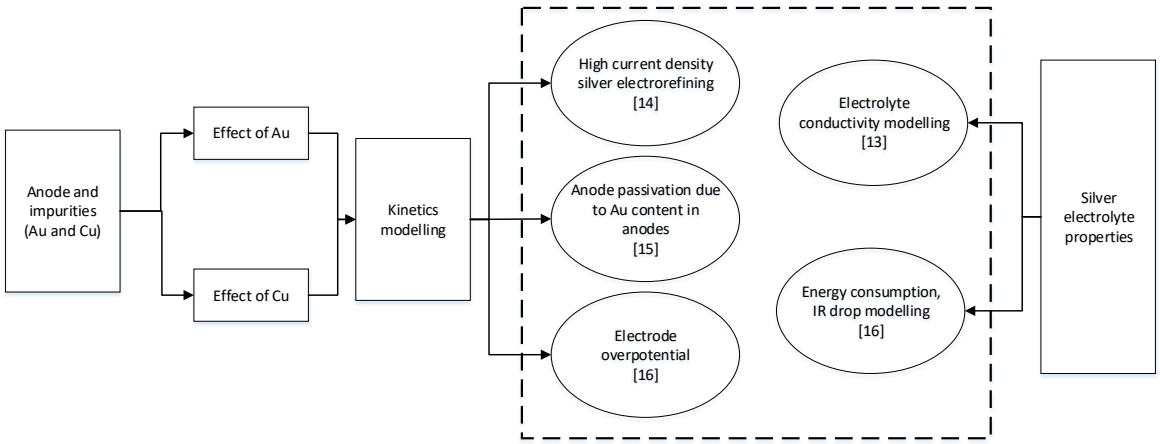

Figure 2. Method of the investigation on the aspects for the high current density (HCD) application (dashed box) is based on the anodic [14–16] and electrolytic [13,16] modelling.

All of the models were constructed with the range of parameters according to the existing industrial practices. Conductivity model was developed with a full factorial design of electrolyte concentrations ($[Ag^+]$, $[Cu^{2+}]$, $[H_2SO_4]$, $[Pb^{2+}]$) and temperature. Measurements were conducted with a Knick Portamess®913 Cond conductivity meter (Knick Elektronische Messgeräte GmbH and Co KG, Berlin, Germany). Meanwhile, the models of silver dissolution and the effect of Au-to-anode passivation were developed from the series of anodic polarization of pure silver and Au-Ag binary alloys with known ranges of Au content. And finally, the electrode overpotential model was developed from galvanostatic measurements with pure silver as working electrode at a current density of 1000 A/m^2. The tests were conducted at different concentrations and temperature of electrolyte. Statistical analysis the developed models has demonstrated that every model presented in [13–16] fulfils the requirements of a good model.

With the strict policy of precious metal refineries, measurements using industrial electrolytes and anodes were not possible. Throughout the study, only a series of industrial tests was conducted in a precious metal refinery to validate the developed the conductivity model from previous study [13] in industrial electrolyte concentration shown in Table 2. The conductivity values measured and calculated by the model for the 20 samples taken at two temperatures of 25 °C and 40 °C. From the validation,

additional models of conductivity were also developed and defined as validation ($\kappa_{validation}$) and industrial ($\kappa_{industrial}$) models. Validation model was developed from the concentration coefficients from the empirical model while the temperature coefficient was taken from the validation results. On the other hand, industrial model was independently developed only from the industrial measurements. The schematic of the conductivity modellings and their correlation are shown in Figure 3.

Table 2. Electrolyte conditions of the industrial practice.

Parameters	$[Ag^+]$, g/dm^3	$[HNO_3]$, g/dm^3	$[Cu^{2+}]$, g/dm^3	$[Pb^{2+}]$, g/dm^3
Values	97.9 ± 8.3	0.3 ± 0.1	56.9 ± 1.9	1.6 ± 0.1

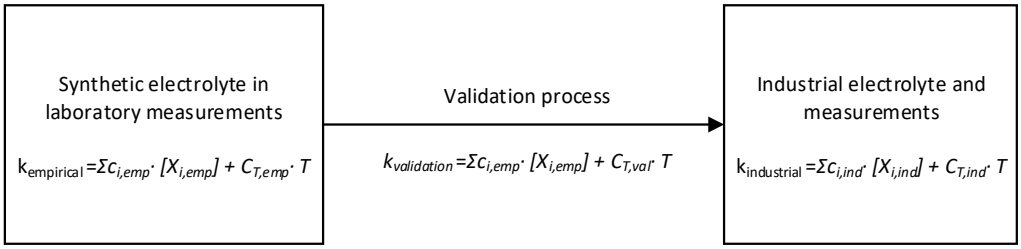

Figure 3. Schematic of the empirical, validation, and industrial models.

All of the developed models were also used as the base to study HCD application with particular attention paid to the cell voltage and specific energy consumption (SEC). Simulations and comparison of HCD and conventional process were conducted based on the electrolyte concentrations from literature. Finally, an optimum condition of HCD silver electrorefining was established in order to have both low energy consumption and low inventory of silver in the electrorefining process.

3. Theoretical Background

The evaluation of optimum parameters was designed mainly based on two calculated outcome of specific energy consumption (SEC) and silver inventory in the process.

3.1. Specific Energy Consumption

Theoretically, the main consumable of an electrorefining process is the electrical energy. With the electrical energy consumption (E_{cons}) outlined in Equation (1), the SEC of a silver electrorefining process is defined as Equation (2) below, where E_{cell} is the cell voltage (V). With the data of the constants (n, F and M_{Ag}) and the current efficiency of conventional process of 92–95% [9,11] and HCD of 98–99% [4], the only variable left from Equation (2) is the cell voltage (V_{cell}).

$$E_{cons}(\text{kWh}) = E_{cell} \cdot I \cdot t \tag{1}$$

$$SEC\left(\frac{kWh}{kg}\right) = \frac{E_{cons}}{m_{Ag}} = \frac{V_{cell} \cdot F \cdot n}{3600 \cdot CE \cdot M_{Ag}}. \tag{2}$$

Cell voltage is the sum of potentials from the process. Excluding the external voltage drops such as busbar or electrical contacts, cell voltage components in silver electrorefining process are voltage drop due to the conductivity of electrolyte, anode polarization with the effect of gold, and cathode polarization. Thus, the cell voltage can be written as Equation (3)

$$V_{cell} = \eta_a + |\eta_c| + \eta_{pass} + IR \tag{3}$$

where η_a is the anodic overpotential, η_c is the cathodic, η_{pass} is the excess polarization due to anode passivation, and *IR* is the potential drop due to electrolyte resistivity. The effect of conductivity to the *IR* drop is shown in Equation (4).

$$IR_{drop} = \frac{I}{A} \cdot \frac{l_{el}}{\kappa} = j \cdot \frac{l_{el}}{\kappa} \tag{4}$$

where I is current (A), l_{ek} is the interelectrode distance (m), A is the surface area (m^2) and κ is the conductivity (S/m).

3.2. Silver Inventory

One of the economic aspects of the silver electrorefining besides the energy consumption is the silver inventory in the process. Silver inventory as the result of HCD can be calculated from the effect of increasing process throughput to the process footprint, in this case the volume of electrolyte. From the Faraday law of electrolysis in Equation (5), the production rate of a plant as function of the electrolyte volume shown in Equation (6)

$$m_{Ag} = \frac{I \cdot t \cdot M_{Ag}}{n \cdot F} \tag{5}$$

$$\frac{m_{Ag}}{t}\left(\frac{kg}{day}\right) = j \cdot \frac{A}{V} \cdot \frac{M_{Ag}}{n \cdot F} \cdot V_{tot} \tag{6}$$

where j is the current density (A/m^2), A/V is the effective surface area of anode to electrolyte volume (m^2/dm^3), M_{Ag} is the molar mass of silver, n is the electron valence of silver, F is Faraday constant and V is the electrolyte volume (dm^3).

4. Results and Discussions

4.1. IR Rrop

Energy consumption in an electrorefining process is mainly due to the resistivity of the electrolyte. To estimate the *IR* drop in this system, an empirical conductivity model based on laboratory measurements shown in Equation (7) was developed and confirmed to be the accurate for the system when electrolyte properties are $[Ag^+]$ of 40–150 g/dm^3, $[Cu^{2+}]$ of 0–80 g/dm^3, $[HNO_3]$ of 0–15 g/dm^3 and T of 25–45 °C [13] and unlike the other models, conductivity modelling of silver electrolyte had been conducted by previous study [17]. Thus, this model was statistically tested and compared to the previous model by Gordon and Davenport [17] and is proven to be a valid model and has better accuracy in comparison to the model of Gordon and Davenport [13].

$$\begin{aligned}\kappa_{empirical} = 10.844 + 0.277 \cdot [Ag^+] + 3.268 \cdot [HNO_3] + 0.700 \cdot \left[Cu^{2+}\right] + 0.204 \\ \cdot \left[Pb^{2+}\right] + 0.573 \cdot T + 0.008 \cdot [Ag^+] \cdot T + 0.049 \cdot [HNO_3] \cdot T + 0.02. \\ \cdot \left[Cu^{2+}\right] \cdot T\end{aligned} \tag{7}$$

In Equation (7) κ is the conductivity of electrolyte (mS/cm) and T is temperature (°C) and concentrations are given as g/dm^3.

Furthermore, validation of the model was conducted and according to the method in Figure 3, the developed validation and industrial models are shown in Equations (8) and (9) respectively. As the industrial model was developed only from the steady condition of industrial electrolyte measurements, the model shows different behavior. As an example, the effect of $[Ag^+]$ is shown to be lower and $[HNO_3]$ has a negative effect to the conductivity.

$$\begin{aligned}\kappa_{validation} = 61.2044 + 0.277 \cdot [Ag^+] + 3.268 \cdot [HNO_3] - 1.648 \cdot T + 0.700 \cdot \left[Cu^{2+}\right] + 0.204 \cdot \left[Pb^{2+}\right] \\ +0.008 \cdot [Ag^+] \cdot T + 0.049 \cdot [HNO_3] \cdot T \\ +0.02 \left[Cu^{2+}\right] \cdot T\end{aligned} \tag{8}$$

$$\kappa_{Industrial} = 114 + 0.11\cdot\left[Ag^{+}\right] - 0.99\cdot[HNO_3] + 0.32\cdot T + 0.025\cdot\left[Cu^{2+}\right] + 2.22\cdot\left[Pb^{2+}\right]. \quad (9)$$

The accuracy of all models to the industrial measurement values are shown in Figure 4. Figure 4a–c show that the empirical model accurately predicts conductivities at lower temperature while at higher temperatures the model over calculates the electrolyte conductivity. Validation model accuracy which is as shown by Figure 4d–e has the improved prediction of conductivity values at higher temperature are closer to the measurements. On the other hand, the goodness of fit (R^2) of the model has become significantly lower as shown by Figure 4f. Finally, the industrial model has the best fit to the measurement values as can be seen in Figure 4g–i. While industrial model is the most representative model for industrial electrolyte, narrow range of the electrolyte concentration creates a challenge for the calculating conductivity of wider range electrolyte concentrations. All models in Equations (7)–(9) were included for further calculation in this study.

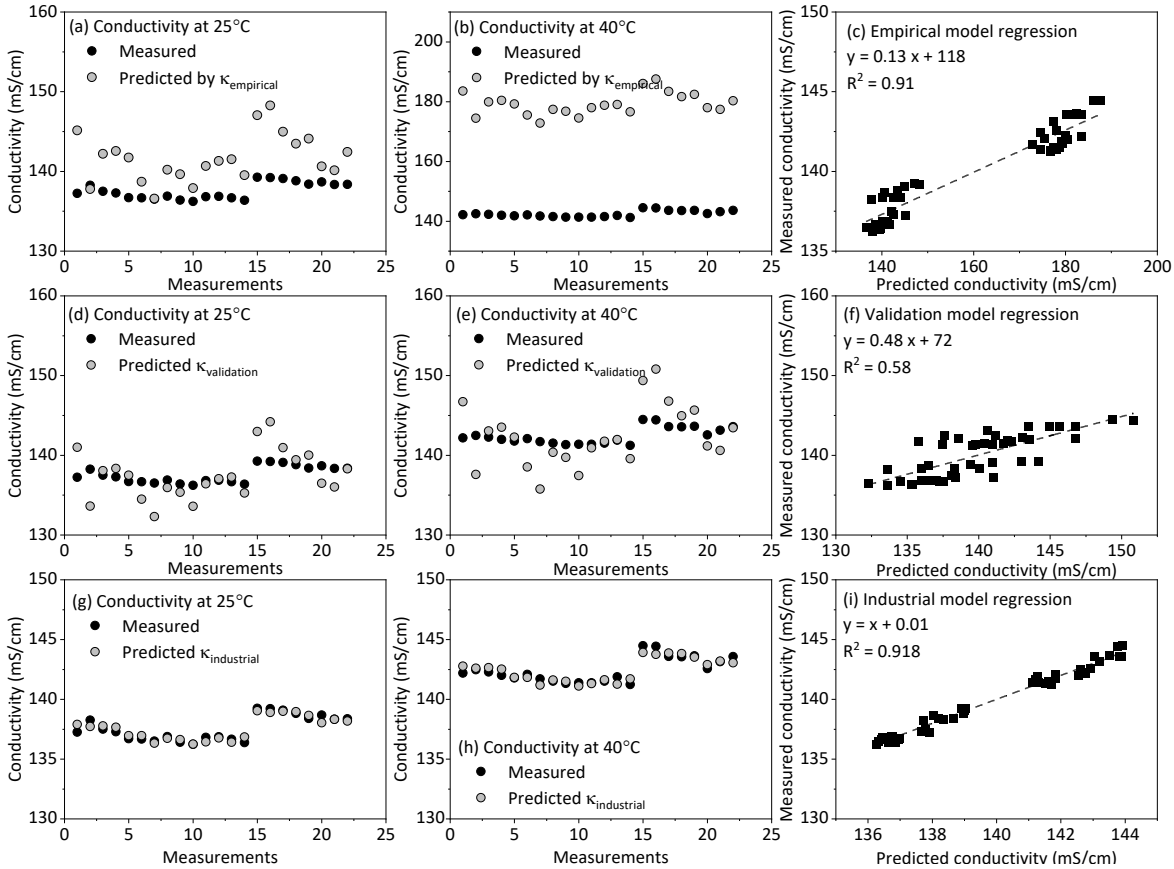

Figure 4. Results of predicted and measured values of empirical model (**a–c**), validation model (**d–f**), and industrial model (**g–i**) for the industrial electrolyte conditions in Table 2.

From the electrolyte concentrations in Table 2, with the exempt of $[Ag^{+}]$, the impact of applying HCD calculated with the three models were simulated with the assumption of industrial current density of 420 A/m^2 and l_{ek} of 5 cm [11] as shown in Figure 5. The simulation of *IR* drop increase as a function of $[Ag^{+}]$ demonstrates the impact of HCD application in the range of $[Ag^{+}]$ from 60–200 g/dm^3.

From the Figure 5, increasing the existing industrial current density to 1000 A/m^2 increases the IR drop significantly from app. 1.6 V calculated by the empirical model to 2 V from the validation and industrial models. The increase accounts for more than 100% of the initial IR drop of the process. The Figure also demonstrates that high $[Ag^{+}]$ is preferred in order to have lower increase of *IR* drop. Another potential factor is the effect of $[Cu^{2+}]$ as it is shown to increase the electrolyte conductivity as shown by all of the models outlined in Equations (7)–(9). In a recent study, having $[Cu^{2+}]$ in electrolyte was also encouraged as the study suggest electrolyte compositions of $[Ag^{+}] > 60$ g/dm^3,

$[Cu^{2+}] < 60$ g/dm^3, and $[HNO_3] < 7$ g/dm^3 [18]. Thus, further simulation of the effect of $[Ag^+]$ and $[Cu^{2+}]$ is required to have an optimum condition of electrolyte for a minimum impact of HCD application due to the increase of *IR* drop.

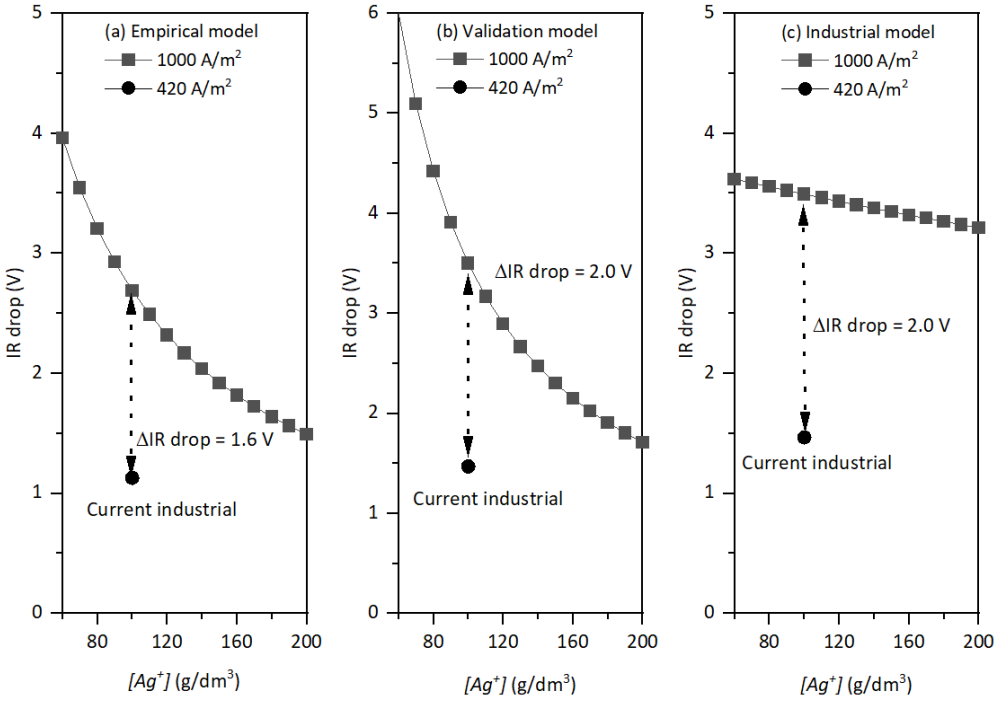

Figure 5. Increase of IR drop for the implementation of HCD operation calculated by (**a**). empirical model, (**b**) validation model, and (**c**) industrial model.

Calculation of the conventional process *IR* drop by using the Equation (4) from the data in Table 1 shows *IR* drop values within the range of 0.8–2.3 V which equal to 55–82% of the total cell potential. As it can be expected, HCD process results in higher cell potential thus the role of electrolyte conductivity is significant. With the positive effect of $[Cu^{2+}]$ to the conductivity of electrolyte, it is important to take a study of the possibility of having $[Cu^{2+}]$ in smaller ratios of $[Cu^{2+}]/[Ag^+]$ to achieve both optimum conductivity and to avoid the co-deposition of Cu on the cathode. A comparison of the $[Cu^{2+}]/[Ag^+]$ levels from previous studies is shown in Table 3.

Table 3. $[Ag^+]$ and maximum $[Cu^{2+}]$ in silver electrolytes.

Concentrations	**[19]**	**[7]**	**[20]**	**[6]**	
$[Ag^+]$	40	150	60–160	65–120	>60
$[Cu^{2+}]$	35	max 45	60	max 50–100	< 60
$[Cu^{2+}]/[Ag^+]$	0.875	0.3	0.5–1	0.77–0.83	0.8–1.3

From the suggested general $[Ag^+]$ of > 60 g/dm^3 [6] and in *HCD* of 100–150 g/dm^3 [4], the *IR* drop values in the range of $[Ag^+]$ of 60–200 g/dm^3 were simulated by using the models in Equations (7)–(9) at the range of $[Cu^{2+}]/[Ag^+]$ as shown in Figure 6 with the constant values of $[HNO_3]$ of 5 g/dm^3 at median temperature of 35 °C.

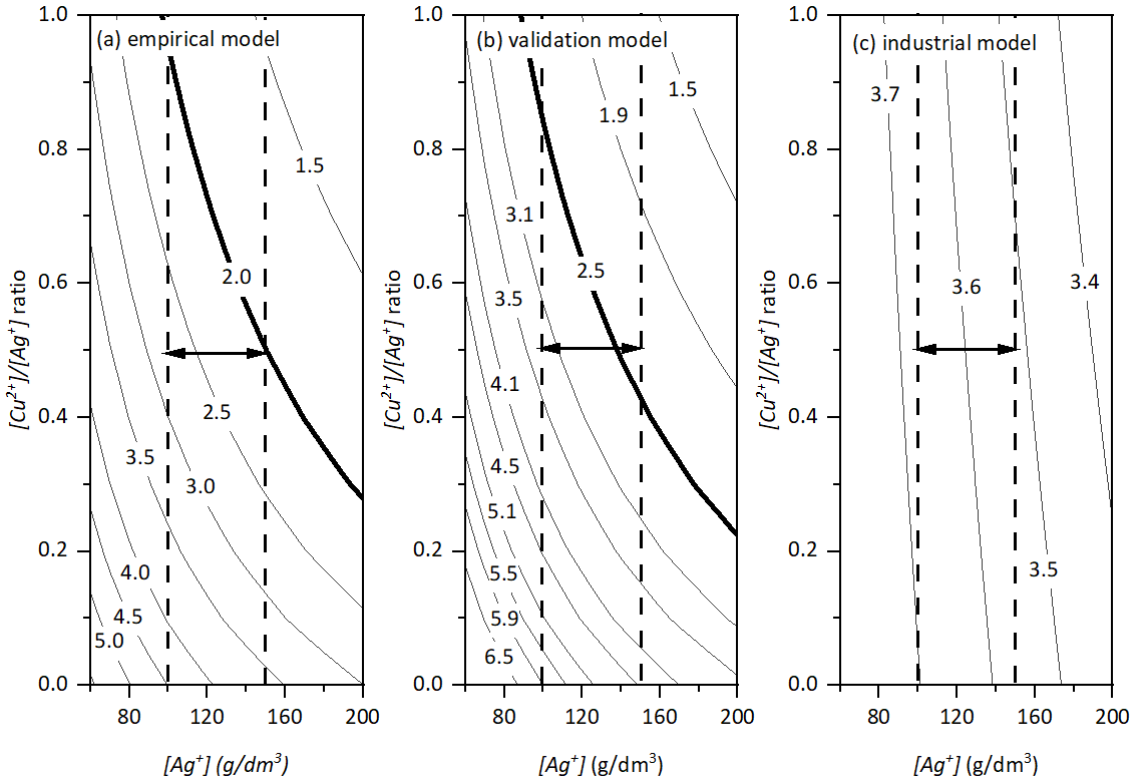

Figure 6. The effect of $[Ag^+]$ and $[Cu^{2+}]$ to the *IR* drop in the application of 1000 A/m^2 current density calculated with (**a**) empirical model, (**b**) validation model, and (**c**) industrial model.

Figure 6a,b show large ranges of *IR* drop and the growing distances between the *IR* contour lines which indicates that as the concentrations of $[Ag^+]$ and $[Cu^{2+}]$ are higher, their effect to *IR* drop reduction becomes insubstantial. As can be seen, in each of both figures, a bold line was added showing the limit where increase of concentrations affect to the reduction of *IR* drop substantially. Meanwhile, Figure 6 c shows narrow *IR* drop range and uniform increase throughout the $[Ag^+]$ levels. In order to set the optimum condition electrolyte, the added dashed lines indicate the range of $[Ag^+]$ within 100–150 g/dm^3 as suggested for HCD operation [4]. From Figure 6 a, the bold line cross the the dashed line at app. 0.9 at 100 g/dm^3 of $[Ag^+]$ and app. 0.5 at 150 g/dm^3 of $[Ag^+]$. With the first value of $[Cu^{2+}]/[Ag^+]$ at 0.9 has high risk of Cu co-deposition, the second value at 0.5 can be taken as the minimum value of the ratio for an optimum HCD.

With the range of $[Ag^+]$ of 100–150 g/dm^3 and $[Cu^{2+}]/[Ag^+]$ of 0.5, the *IR* drop values for 1000 A/m^2 operation based on the models in this study are shown in Table 4. In the table, the empirical model shows the lowest *IR* drop calculation while the industrial model has the highest value.

Table 4. Optimum $[Ag^+]$ and $[Cu^{2+}]$ in silver electrolytes for HCD silver electrorefining operation.

Level	$[Ag^+]$, g/dm^3	Optimum $[Cu^{2+}]/[Ag^+]$	$[Cu^{2+}]$, g/dm^3	IR Drop (V)		
				Empirical	Validation	Industrial
Min $[Ag^+]$	100	0.5	50	2.75	3.24	3.67
Max $[Ag^+]$	150	0.5	75	2.05	2.30	3.52

As can be seen from Table 4, the difference of empirical with the industrial conductivity values is significant. This was mainly caused by the actual concentration of the industrial electrolyte where more dissolved contents were presents, while the empirical model was built only with the effect of major concentrations such as $[Ag^+]$, $[HNO_3]$, $[Cu^{2+}]$, and $[Pb^{2+}]$. Validation model connects empirical and industrial model with the correlation schematically shown in Figure 3. As mentioned in Section 2,

the validation tests were conducted to a type of industrial electrolyte only, thus the model has questionable validity to be applied in different types of electrolyte. With these weakness of each model in correlation to the range industrial application, all the models were taken into account in predicting the outcome in terms of specific energy consumption of HCD in the suggested electrolyte condition from this study.

4.2. Anodic and Cathodic Overpotential (η_a and η_c)

From the modelling of the galvanostatic results [15], cathodic overpotential when operating at 1000 A/m^2 current density could not be measured and modelled reliably due to the dendritic deposition, nevertheless the measured cathodic overpotentials were 147–297 mV and decreasing with increasing silver concentration. The anodic overpotential at 1000 A/m^2 as function of electrolyte conditions was modelled as follows:

$$\eta_a = 452.8 - 1.14 \cdot \left[Ag^+\right] - 5.31 \cdot [HNO_3] - 1.21 \cdot \left[Cu^{2+}\right] - 4.13 \cdot T \quad (10)$$

where η_a is the anodic overpotential (mV), concentrations in g/dm^3 and temperature in degrees centigrade. Using the electrolyte concentrations in Table 4, the anodic overpotential is within the range of 20–107 mV.

Anodic Tafel slope (b_a) model of Ag in $AgNO_3$-HNO_3 from the study of Ag kinetic dissolution [14] can be written as Equation (11) with model accuracy shown in Figure 7a, while the difference of both values are shown in Figure 7b. As can be seen from the model and measurements, the anodic Tafel slope is within the range of 0.24–0.45 V. Thus, by using the correlation of current density and anodic overpotential outlined in Equation (12), increase of current density from 420 A/m^2 to 1000 A/m^2 requires small increase of anodic overpotential of 0.09–0.2 V. This suggests that increasing current density to 1000 A/m^2 does not increase the anodic overpotential substantially.

$$b_a = 0.7 - 0.002 \cdot \left[Ag^+\right] - 0.01 \cdot [HNO_3] - 0.0037 \cdot T \quad (11)$$

$$\Delta\eta_a = b_a \log\left(\frac{i_2}{i_1}\right) \quad (12)$$

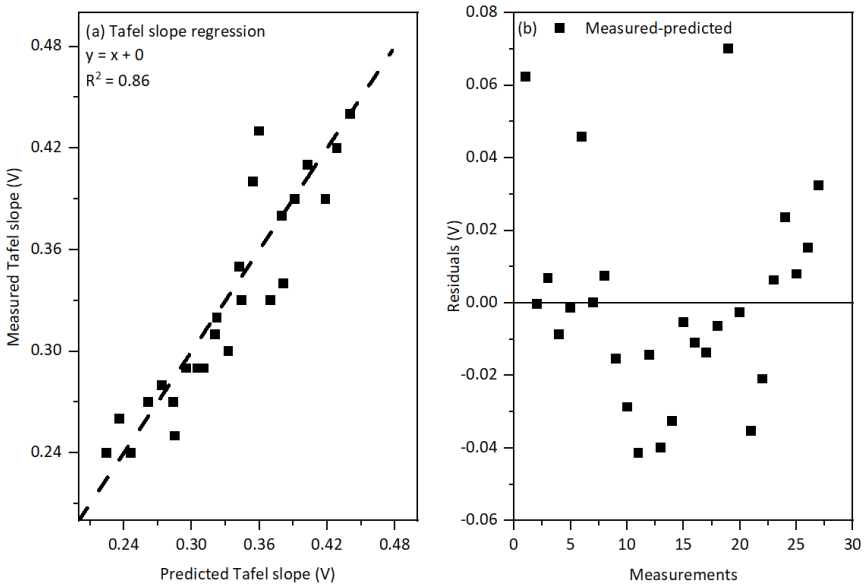

Figure 7. (**a**) Predicted vs measured of anodic Tafel slope values of Ag in $AgNO_3$-HNO_3 electrolyte and (**b**) residual values of the prediction to the measurements results.

4.3. Passivation Overpotential (η_{pass})

Gold in silver anodes causes anode passivation. This is due to anode surface enrichment by gold along silver dissolution. In earlier studies, application of HCD in high $[Ag^+]$ electrolyte (min 100 g/dm^3) was shown to be kinetically efficient for maximum Au content less than 6% in the anode [15]. The passivation range due to Au content in anode can be calculated by using Equation (13) [16].

$$\eta_{Au} = 11.25 + 1.01\ wt\%_{Au} - 0.09\left[Ag^+\right] - 0.60[HNO_3] + 0.38\ T. \quad (13)$$

With the limitation of Au content to maximum of 6%, the effect of passivation overpotential is minimized when using the electrolyte concentrations in Table 4. This results in passivation overpotential of 0.2 V.

4.4. Circulating Electrolyte volume

For the value of *A/V* set to a constant of 0.004, 1 m^2 of anode surface per 250 dm^3 of bulk electrolyte, taken from the general industrial practices for Moebius cell [11]. At the rate of production of 100 kg/day, electrolyte volume as a function of applied current density is shown by Equation (14).

$$V_{tot}\left(dm^3\right) = \frac{2.59{\cdot}10^5}{j\left(\frac{A}{m^2}\right)}. \quad (14)$$

From above equation, to have the same productivity, higher current density process requires smaller volume of electrolyte.

4.5. Cell Voltage, SEC, and Silver Inventory

For summary, the electrolyte concentrations in Table 4 resulted in the total cell voltage components as follow:

- *IR* drop
  - Empirical model = 2.05–2.75 V
  - Validation model = 2.30–3.24 V
  - Industrial model = 3.52–3.67 V
- η_a and η_c = 0.32–0.40 V
- η_{Au} = 0.02 V

As can be seen from the components above *IR* drop is the most dominant by contributing 86–91% of the cell voltage. This was further supported by the anodic Tafel slope model which shows that increase of current density insubstantially affects the anodic overpotential.

The increasing portion of *IR* drop to the cell voltage were simulated as shown in Figure 8. The contribution of *IR* drop to cell voltage increases with increase in current density and *IR* drop contributes more than 85% of the cell voltage at 1000 A/m^2 operation. In addition, operating at lower range of electrolyte concentration increases the *IR* drop portion to more than 90% of the cell voltage for electrolyte with lower $[Ag^+]$. From the simulation, increase of electrolyte concentrations reduce the *IR* drop portion of cell voltage significantly while increase of temperature is shown to have less impact. While *IR* drop can be reduced by increasing both temperature and concentrations of the electrolyte, it cannot be avoided that *IR* drop contribution to cell voltage at 1000 A/m^2 is significant as calculated by all the models of the current study.

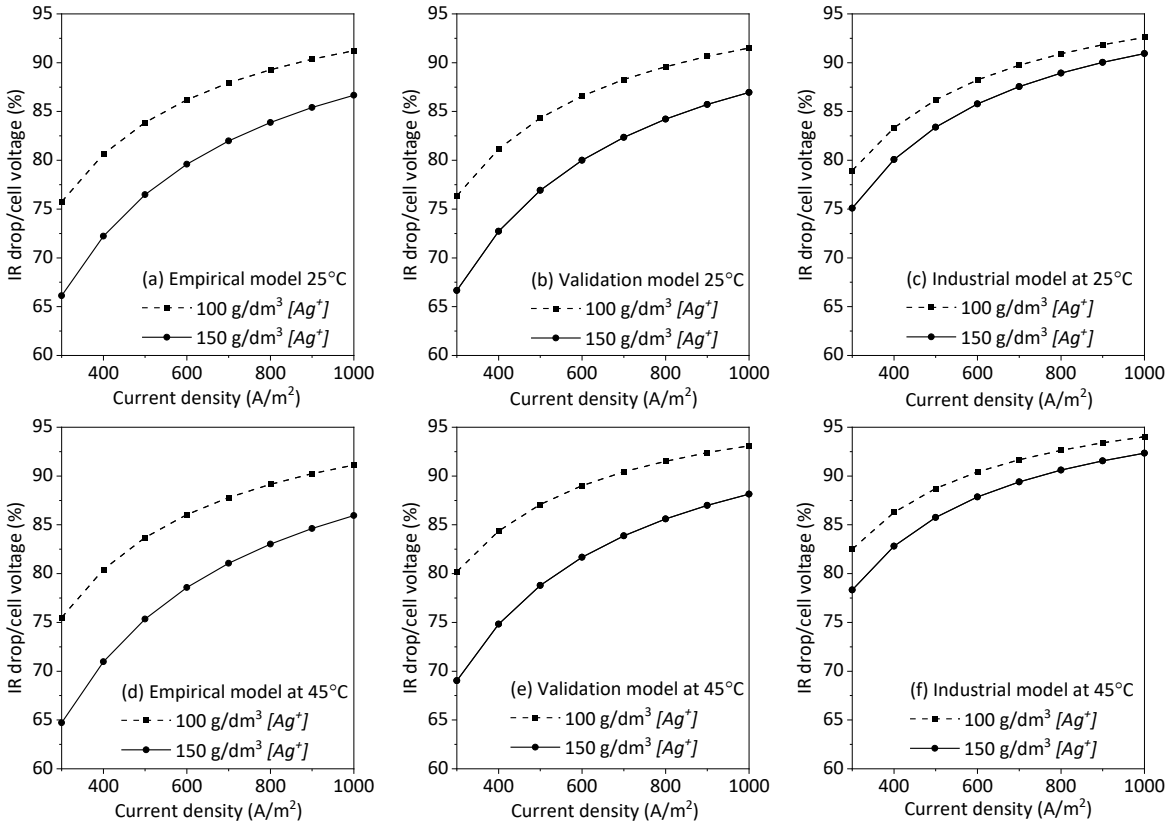

Figure 8. *IR* drop and cell voltage calculation for the electrolyte concentrations shown in Table 4.

Towards the potential application of HCD as an improvement to the current silver electrorefining practices, competitiveness of the process key figures in comparison to the conventional process is of importance. Accordingly, the key figures of both processes are outlined in Table 5. The suggested parameters from this study are compared to the HCD from previous publication [4] and to the conventional silver electrorefining [7–12].

Table 5. Specific energy consumption (SEC) and silver inventory comparison of HCD and conventional silver electrorefining.

Parameters	*HCD* in This Study	HCD from Previous Study [4]	Conventional Silver Electrorefining [7–12]
$[Ag^+]$ (g/dm^3)	100–150	100–150	30–150
$[Cu^{2+}]$ (g/dm^3)	50–75	n.a	45–100
$[HNO_3]$ (g/dm^3)	5–7	n.a	0–10
T (°C)	35–45	<55°C	25–50
Current density (A/m^2)	1000	1000	200–500
Cell voltage (V)			
a) Empirical model b) Validation model c) Industrial model	a) 2.39–3.09 b) 2.64–3.58 c) 3.86–4.01	<5 V	1.5–2.8
Current efficiency (%)	98–99 [4]	98–99	92–95
SEC (kWh/kg)			
a) Empirical model b) Validation model c) Industrial model	a) 0.60–0.78 b) 0.67–0.90 c) 0.98–1.01	1.27–1.28 *	0.44–0.76
Comparisons based on 100 kg of Ag product / day			
Electrolyte volume (dm^3)	259	259 *	518–1295 *
Silver inventory (kg)	25.9–38.85	25.9–38.85 *	15.54–194.25 *

* calculated from the data in the references.

Table 5 shows that HCD in this study has competitive advantage in comparison to both previous HCD and conventional silver electrorefining process. When the current density of HCD is increased to more than double of the conventional process, the cell voltage is shown to increase only for 30–40%. This increase of SEC is a significant improvement from the 1.27–1.28 kWh/kg from the previous HCD [4] which accounts more than 60% increase of SEC in comparison to the conventional process. With the same $[Ag^+]$ level, the utilization of $[Cu^{2+}]$ an $[HNO_3]$ to boost the conductivity was the cause of significantly lower SEC.

From Table 5, electrolyte volume and silver inventory were calculated for the same throughput. Comparison of HCD to the conventional process on the basis of 100 kg/day production rate shows that the median value of HCD silver inventory of approximately 32 kg which is far less than the median value of approximately 105 kg of the conventional process [7–12]. The required electrolyte volume of HCD was also shown to be less than half of the conventional process. Thus, the HCD application could turn to be highly beneficial as it is not only increasing the capacity due to the high throughput of the process but also has the possibility to reduce the process inventory and the equipment footprint. This suggests feasibility also from the economic point of view of the process.

5. Conclusions

This study simulates the impact of HCD, 1000 A/m^2 current density operation in silver electrorefining through the optimization of the electrolyte composition. With the objective to increase the applicability and competitiveness of HCD in comparison to the conventional process, an optimum range of electrolyte composition was developed through simulation. With the prudential practice of precious metal refineries, the study has the limitation in the measurements of industrial electrolytes and anodes with only a validation of conductivity model was conducted. Therefore, this study was mainly focused on the simulation of the developed models from previous publications.

From the simulation, it was found that by increasing the electrolyte conductivity through the introduction of $[Cu^{2+}]$ would lower the cell voltage from the *IR* drop significantly. While conductivity is in general an important property in electrorefining process, the higher current density in an HCD operation amplifies the significance of IR drop. Its contribution to cell voltage increased to more than 85% which is higher than the 55–82% range in the conventional process. The optimum concentrations for HCD electrolyte were suggested being within the range of 100–150 g/dm^3 for $[Ag^+]$ and 50–75 g/dm^3 for $[Cu^{2+}]$. While increasing electrolyte silver and copper concentrations reduce the IR drop substantially, the effect of temperature is shown to have less impact. As a conclusion, HCD operation in the suggested electrolyte results in 0.60–1.01 kWh/kg of SEC with silver inventory in the electrolyte within the range of 25.9–38.85 kg for a 100 kg/day production rate. While this study elaborated the potential improvement of silver electrorefining process, study of the economic and environmental impact of HCD will add values to this process improvement.

Author Contributions: A.T.A. and J.A. performed the experiments, data analysis and wrote the paper. M.L. reviewed the paper and provided the research funding and resources. All authors have read and agreed to the published version of the manuscript.

Funding: Symmet project (project number of 2117441).

Conflicts of Interest: The authors declare no conflict of interest.

References

1. Habashi, F. *Handbook of Extractive Metallurgy: Volume III Part 6: Precious Metals*; Wiley-VCH Verlag-GmbH: Weinheim, Germany, 1998.
2. The Silver Institute. World Silver Surveys. Available online: https://www.silverinstitute.org/all-world-silver-surveys/ (accessed on 1 April 2020).
3. Mostert, P.J.; Radcliffe, P.H. Recent advances in gold refining technology at Rand Refinery. *Dev. Miner. Process.* **2005**, *15*, 653–670. [CrossRef]
4. Maliarik, M.; Johansson, K.Å.; Ögren, B.; Berg, G.; Johansson, C.D.; Lindh, R.; Ludvigsson, B. High current density silver electrorefining process: Technology, equipment, automation and Outotec's Silver Refinery Plants. In Proceedings of the 7th International Symposium of Hydrometallurgy, Victoria, BC, Canada, 22–25 June 2014; Volume 2, pp. 91–100.
5. Jaskula, M.; Kammel, R. Untersuchungen zur Verbesserung des Platinmetalausbringens bei der industriellen Silberraffination. *Metall* **1997**, *51*, 393–400.
6. Pophanken, A.K.; Friedrich, B.; Koch, W. Challenges in the Electrolytic Refining of Silver–Influencing the Co-Deposition through Parameter Control. *Rare Metal Technol.* **2017**, *2*, 327–380.
7. Leigh, A.H. Precious metals refining practice. In Proceedings of the 2nd International Symposium on Hydrometallurgy, Chicago, IL, USA, 25 February–1 March 1973; pp. 95–110.
8. Pletcher, D.; Walsh, F.C. *Industrial Electrochemistry*, 2nd ed.; Springer: Dordrecht, The Netherlands, 2012; pp. 238–242. [CrossRef]
9. Cornelius, G. Die Raffination von Gold und Silber durch Elektrolyse. In *Elektrolyse der Nichteisenmetalle: 11. Metallurgisches Seminar GDMB*; Verlag Chemie: Weinheim, Germany, 1982; Volume 37, pp. 215–226.
10. Shibasaki, T.; Tsubogami, H.; Nozaki, M. Recent Improvements in Silver Electrolysis at Mitsubishi's Osaka Refinery. In Proceedings of the Precious Metals'89, TMS conference, Las Vegas, NV, USA, 27 February–2 March 1989; pp. 419–430.
11. Mantell, C.L. *Industrial Electrochemistry*, 2nd ed.; McGgraw-Hill: New York, NY, USA, 1940; pp. 253–254.
12. Brumby, A.; Braumann, P.; Zimmermann, K.; van den Broeck, F.; Vandevelde, T.; Goia, D.; Renner, H.; Schlamp, G.; Zimmermann, K.; Weise, W.; et al. Silver, silver compounds, and silver alloys. In *Ullmann's Encyclopedia of Industrial Chemistry*; Wiley-VCH Verlag GmbH & Co. KGaA: Weinheim, Germany, 2012; pp. 42–43.
13. Aji, A.T.; Kalliomäki, T.; Wilson, B.P.; Aromaa, J.; Lundström, M. Modelling the effect of temperature and free acid, silver, copper and lead concentrations on silver electrorefining electrolyte conductivity. *Hydrometallurgy* **2016**, *166*, 154–159. [CrossRef]

14. Aji, A.T.; Aromaa, J.; Wilson, B.P.; Mohanty, U.S.; Lundström, M. Kinetic Study and Modelling of Silver Dissolution in Synthetic Industrial Silver Electrolyte as a Function of Electrolyte Composition and Temperature. *Corros. Sci.* **2018**, *138*, 163–169. [CrossRef]
15. Aji, A.T.; Halli, P.; Guimont, A.; Wilson, B.P.; Aromaa, J.; Lundström, M. Modelling of silver anode dissolution and the effect of gold as impurity under simulated industrial silver electrorefining conditions. *Hydrometallurgy* **2019**, *189*, 105105. [CrossRef]
16. Aji, A.T.; Aromaa, J.; Lundström, M. Specific Energy Consumption Modelling of Silver Electrorefining. In Proceedings of the European Metallurgical Conference (EMC), Dusseldorf, Germany, 23–26 June 2019; Volume 2, pp. 807–820.
17. Gordon, N.L.; Davenport, W.G. Electrical conductivities, densities and viscosities of silver refining electrolyte. *Can. Min. Q.* **1981**, *20*, 369–372. [CrossRef]
18. Maurell-Lopez, A.K. *Verhalten von Kupfer und Palladium bei der Raffinationselektrolyse von Recycling-Silber*; Shaker Verlag GmbH: Düren, Germany, 2017; ISBN 978-3-8440-5987-8.
19. Johnson, O. Refining processes. In *Silver: Economics, Metallurgy, and Use*; Butts, A., Coxe, C.D., Eds.; Van Nostrand Company, Inc.: Princeton, NJ, USA, 1967; Chapter 5.
20. Hunter, W. Electrolytic Refining. US Patent no. 3,975,244, 17 August 1976.